J. Phys.: Condens. Matter **22** (2010) 084012 (12pp) doi:10.1088/0953-8984/22/8/084012

UV photo-dissociation and photodesorption of N_2O on Ag(111)

Ki Hyun Kim[1], Kazuo Watanabe[1], Dietrich Menzel[1,2] and Hans-Joachim Freund[1]

[1] Fritz-Haber-Institut der Max-Planck-Gesellschaft, Faradayweg 4-6, 14195 Berlin, Germany
[2] Physik-Department E20, Technische Universität München, 85748 Garching, Germany

E-mail: watanabe@fhi-berlin.mpg.de

Received 3 August 2009, in final form 10 September 2009
Published 4 February 2010
Online at stacks.iop.org/JPhysCM/22/084012

Abstract

Nanosecond laser induced photoreactions of N_2O adsorbed on Ag(111) have been studied by temperature programmed desorption (TPD) and mass-selected, angle-dependent time-of-flight (MS-TOF) measurements of neutral desorbing particles. N_2O molecules in the first monolayer are thermally inert but photo-dissociate into $N_2 + O$, or photodesorb molecularly or dissociatively, at photon energies above 3.5 eV. We have found that TOF spectra of photodesorbed N_2 as well as of N_2O measured at $h\nu = 4.7$ eV consist of two velocity components. The desorption flux of the fastest component of N_2O peaks $\sim 25°$ off the surface normal, whereas the others are directed in the surface normal. Origins and photo-excitation as well as photodesorption mechanisms of the N_2O and N_2 signals are discussed.

(Some figures in this article are in colour only in the electronic version)

1. Introduction

N_2O is known as an important intermediate in automobile catalysts for NO_x reduction to form N_2. Molecular-level studies have been performed in catalytic NO decomposition on Pd(110) [1], Rh(110) and Rh(111) [2], and TiO_2(110) [3], for example. On these surfaces thermal dissociation of N_2O is found. On Pt(111), on the other hand, N_2O is not dissociated thermally [4] but photo-dissociates at photon energies exceeding 4.35 eV [5], which has been explained by the substrate mediated excitation mechanism [6].

Photochemistry of N_2O on Ag(111) has not been reported so far, but electron stimulated dissociation of multilayer N_2O to form desorbing N_2 and oxygen adatoms was reported by Schwaner *et al* [7]. They concluded that the reaction is induced by the attachment of secondary electrons produced by the primary electron beams (50 and 2500 eV), via transient N_2O^- formation. In the monolayer regime, neither dissociation nor desorption of N_2O was observed; they ascribed this to the strong quenching of anions formed by electron attachment and of cations formed by impact ionization.

Interestingly, N_2O is formed photochemically [8] as well as thermally [9, 10] from NO dimers on Ag(111). Recently, we found that not only N_2O but also N_2 is formed from the NO dimers under irradiation by 2.3–4.7 eV photons, and that the photoproducts N_2 and N_2O desorb with very different translational temperatures (T_ts) of 5700 and 1200 K, respectively [11]. In order to distinguish whether the energetic N_2 is formed via photo-dissociation of an intermediate N_2O or produced directly from the NO dimer, we have now studied the photochemistry of pure N_2O adsorbed on clean Ag(111) in the monolayer regime, using UV laser excitation. We find surprising complexity of the photo-induced processes when analyzing detailed desorption parameters. The N_2O adsorbate undergoes photoreactions at $h\nu \geqslant 3.5$ eV where N_2O either photodesorbs molecularly or photo-dissociates into N_2 and O; the formed N_2 is also photodesorbed. The photo-excitation mechanisms are studied by light polarization and incident angle dependences of photodepletion cross sections. Furthermore, the photodesorption dynamics of N_2O and N_2 are investigated by angle-resolved, mass-selected time-of-flight (MS-TOF) measurements. We find that there are at least two components with different T_ts and different angular distributions for both photodesorbing N_2 and N_2O, in spite of the fact that the temperature programmed desorption (TPD) results show only a single peak of simple shape for the N_2O monolayer before irradiation. Also, a very fast change in the adsorbate layer induced by irradiation is seen when following the N_2 signal. We interpret this as evidence that more than one

interconverting adsorbate species and both direct and indirect excitation mechanisms are involved in the photodesorption of N_2O.

2. Experiment

All experiments were performed in an ultrahigh vacuum system (base pressure $<10^{-10}$ mbar) consisting of two chambers for sample preparation and measurements, which has been briefly described previously [12, 13]. A single crystal Ag(111) sample (10 mm in diameter, 2 mm thick) was used as the substrate; it could be cooled to below 30 K by liquid helium as well as heated in a controlled way by electron bombardment from the backside of the crystal. Monolayers of N_2O on Ag(111) were used for all the experiments. They were prepared by dosing the sample surface at 71 K with N_2O gas from a pulsed valve through a copper tube (inner diameter $\sim$ 6 mm) ending about 3 cm in front of it. The gas dosage was controlled by the number of valve openings, such that the TPD peak from the first monolayer was saturated as far as possible, but at the same time preventing any contribution from multilayers. In view of the closeness of desorption from the first and second monolayers, this probably means that the first monolayer was close to saturation, but not fully saturated. Thermally desorbing molecules were detected by a differentially pumped quadrupole mass spectrometer (QMS; Hiden HAL/3F RC 301 PIC) behind a 2 mm skimmer placed 1 mm in front of the surface. The heating rate for TPD was set at 0.5 K s^{-1}. During TPD measurements the sample was biased at -100 V to avoid electron bombardment from the QMS filament.

For photoreaction measurements the sample surface was cooled to below 30 K and irradiated with nanosecond pulses of the third (355 nm, 3.5 eV) or the fourth (266 nm, 4.7 eV) harmonics of a Nd:YAG laser (Spectra Physics GCR-190), or from a XeCl excimer laser (308 nm, 4.0 eV, Coherent Lambda Physik LPX140i) operating at 10 Hz. The polarization of the light from the former was chosen by rotating the housing of the higher harmonic generator; usually p-polarized light was used except when noted otherwise. The light from the latter was not polarized. The output beam (diameter $\sim$ 10 mm) of the Nd:YAG laser was cut to a diameter of 7 mm by an iris after being expanded threefold by a telescope to obtain a nearly homogeneous beam spot from the center part of the Gaussian profile. The laser beams were directed into the UHV chamber through a MgF viewing port with known transparencies. The typical laser fluence was about 1 mJ cm^{-2}, which ensures the absence of nonlinear effects. Also, heating of the sample by laser irradiation was negligible. The sample temperature during irradiation was kept below 30 K.

Photodesorbed molecules were detected by a QMS (Balzers QMS311) with a LN_2 cooled ionizer to reduce background gases. The flight length L of neutral desorbates, the distance between the sample surface and the exit of the QMS ionizer, was $\sim$19 cm and the solid angle of detection was 0.011 sr. TOF spectra were recorded by a multichannel scaler (MCS; FAST p7882, dwell time 2 μs) triggered by the photodesorption laser. The MCS memory was swept for each laser shot; a TOF spectrum was acquired for every photodesorption event in order to follow the time evolution of not only the TOF spectrum but also the total photo-induced desorption (PID) yield which was obtained by integrating the spectra. However, in order to get signals with a good signal/noise ratio a number of shots had to be accumulated for TOF spectra.

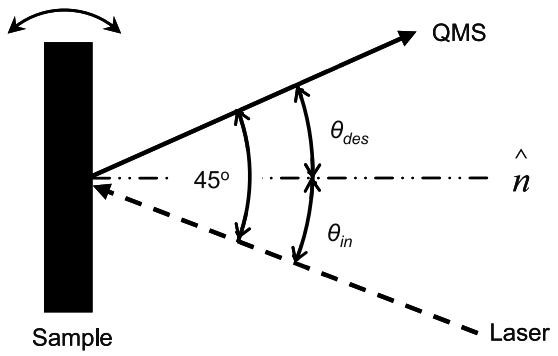

Figure 1. Configuration of MS-TOF and PID measurements. The angle between the QMS and laser beam is fixed at 45°. The direction of the surface normal is varied in the experiment by rotating the sample manipulator.

Angular dependences of the photodesorption cross section (PCS) and the TOF spectrum of photodesorbing molecules were measured by rotating the sample at the crossing point of the laser beam and the QMS center axis. The measurement configuration is schematically drawn in figure 1. A fixed angle of 45° between the laser beam and the QMS axis was imposed by the chamber. Thus, the desorption detection angle $\theta_{\rm des}$ and the light incident angle $\theta_{\rm in}$ with respect to the surface normal could be varied under the constraint $\theta_{\rm des} = 45° - \theta_{\rm in}$. While it is a drawback that both parameters cannot be changed independently, information on the photo-excitation mechanisms and desorption dynamics was still obtainable, as will be described below. The data were normalized with respect to relative sensitivities of the QMS for the target molecules (here N_2O and N_2) after subtracting the contribution to the N_2^+ ($m/e = 28$) signal from N_2O^+ ($m/e = 44$) cracking in the QMS ion source. Also, the change of the irradiated area on the sample surface by rotation was taken into account for the normalization.

3. Results and discussion

3.1. Pre- and post-irradiation TPD of N_2O on Ag(111)

Adsorption states of N_2O and their changes by photo-irradiation have been studied by TPD. Figure 2 displays pre- and post-irradiation TPD results at mass numbers (a) $m/e = 44$, (b) $m/e = 28$, and (c) $m/e = 32$ from a monolayer of N_2O on Ag(111). For the latter, the sample was irradiated with 5000 laser shots ($\sim$1 mJ cm^{-2} per shot) of 3.5, 4.0, or 4.7 eV photons at $\theta_{\rm in} = 45°$. The pre-irradiation TPD spectrum

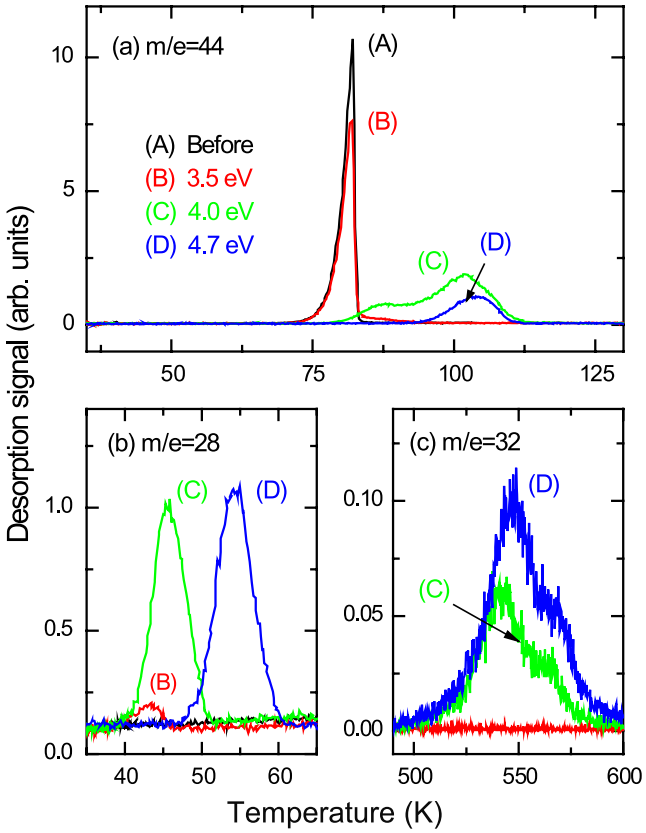

Figure 2. TPD results from Ag(111) dosed with N_2O at 71 K to monolayer saturation before and after irradiation, measured at mass numbers (a) $m/e = 44$, (b) 28, and (c) 32.

(trace A) at $m/e = 44$ shows only a single peak at ∼82 K corresponding to molecular desorption of N_2O from the first monolayer. The monolayer peak shape indicates zeroth order desorption. Analysis of the leading edge which yields a linear Arrhenius plot over most of the peak results in a desorption energy of about 25 kJ mol^{-1}, which is close to the evaporation energy of N_2O [14].

Irradiation by 5000 shots (close to 10^{19} photons cm^{-2}) of 3.5 eV photons (trace B) reduced the N_2O peak to ∼80% without any shift and produced a small tail up to 95 K. After irradiation with 4.0 eV (trace C) and 4.7 eV (trace D) photons, the main peak disappeared and small new peaks of complex shape mostly above 100 K appeared. This must mean that 3.5 eV photons remove some of the N_2O coverage with little production of new species, while at higher photon energies the original N_2O layer is removed and some considerably changed N_2O species remain. The latter changes are probably due to the influence of co-adsorbed fragments, i.e. atomic oxygen and/or N_2 (see below); a contribution of recombination of fragments to the TPD signal is also conceivable.

Before irradiation, no products such as N_2 ($m/e = 28$) and O_2 ($m/e = 32$) were observed in TPD (figures 2(b) and (c)), indicating that N_2O desorbs thermally from Ag(111) without dissociation. This is consistent with previous work [7]. After irradiation with photons ⩾3.5 eV N_2 peaks (very small at 3.5 eV) appeared below 60 K. Also, a (small) recombinative desorption peak of O_2 around 540 K was observed after 4.0 and 4.7 eV irradiation (figure 2(c)). For 3.5 eV, the O_2 peak was not detected, probably because of too low a reaction or detection yield, and/or diffusion into the bulk, of oxygen atoms. These results indicate that N_2O is readily photo-dissociated at 4.0 and 4.7 eV; very little dissociation happens at 3.5 eV. Other possible reaction products, e.g. NO ($m/e = 30$) or NO_2 ($m/e = 46$), were not observed in either pre- or post-irradiation TPD.

3.2. Mass-selected time-of-flight measurements of photodesorbed N_2O and N_2

Direct detection of photodesorbed species yielded signals of N_2O and N_2. They were investigated by angle-resolved MS-TOF measurements. Figure 3 shows TOF spectra of (a) N_2O ($m/e = 44$) and (b) N_2 ($m/e = 28$) photodesorbed from a monolayer of N_2O on Ag(111) measured at desorption angles $\theta_{des} = -25°$, 0°, 25°, and 45° by 4.7 eV photons in p-polarization. These angles have been selected because the first and the last vary the E-vector orientation extremely (predominantly p-polarization and pure s-polarization, respectively); the first and the third vary the polarization but not the detection angle; and the second tests detection in the surface normal, with mixed polarization. Here the desorption signals were accumulated until they had almost leveled off, i.e. the signals correspond to an integral over the entire initial coverage; the necessary irradiances were about 1×10^{18} photons cm^{-2}. The traces in figure 3(b) were obtained from the QMS signal at $m/e = 28$ after subtracting the cracking contribution from N_2O ($m/e = 44$). Also, the intensities of the N_2 and N_2O signals were corrected by taking into account the relative sensitivity of the QMS. Then, the data were further normalized by the percentage of the sample surface irradiated with the laser beam.

All spectra were fitted by a sum of three modified flux-weighted Maxwell–Boltzmann functions for each mass number, $F(t) = \sum_{i=1}^{3} a_i t^{-4} \exp(-b_i(Lt^{-1} - v_i))$, in which a_i, b_i, and v_i are the parameters for amplitude, spread, and shift from Maxwellian, respectively, and L is the distance from the surface to the detector. The data were globally fitted; common parameters b_i and v_i were shared by the data sets at all the desorption angles. Only the parameter a_i was optimized independently for each angle. This fitting procedure should give information about the angular distribution of each speed component.

We focus on the fastest and the medium components (indicated in figure 3 as P_1 and P_2 for N_2O and Q_1 and Q_2 for N_2). The T_is of these components are obtained as 3100, 1100, 2200, and 600 K, respectively. The slowest component in both cases (T_is are 70 K and 60 K for N_2O and N_2, respectively) is attributed to secondary processes such as collisions among adsorbates/desorbates or with the chamber walls.

The TOF spectra of N_2O in figure 3(a) show distinct desorption angle dependences. The P_1 intensity is larger at $\theta_{des} = \pm 25°$ than at $\theta_{des} = 0°$, indicating that P_1 is peaked off-normal. On the other hand, the P_2 intensity is strongest at $\theta_{des} = 0°$. The P_1 to P_2 ratio is almost the same at $\theta_{des} = \pm 25°$, indicating an overriding influence of the desorption angle in

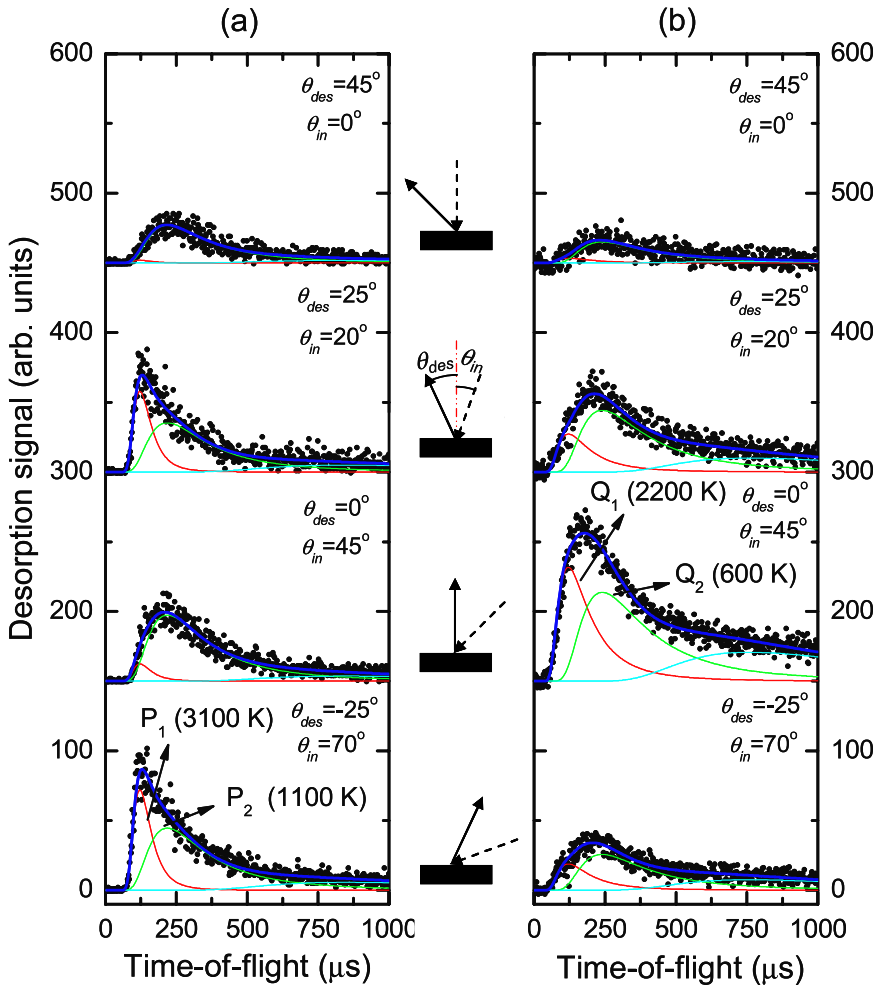

Figure 3. TOF spectra of (a) N_2O and (b) N_2 photodesorbed from the N_2O monolayer on Ag(111) measured at desorption angles $\theta_{\rm des} = -25°$, 0°, 25°, and 45° ($\theta_{\rm in} = 70°$, 45°, 20°, and 0°) from the bottom, by 4.7 eV photons in p-polarization. The spectra are fitted by a sum of three shifted Maxwell–Boltzmann functions. The sum (thick solid curves), the fast component (denoted as P_1 for N_2O and Q_1 for N_2), the medium component (denoted as P_2 for N_2O and Q_2 for N_2), and the slow component (secondary processes) are shown. The desorption and light incident angles are shown schematically as solid and dashed arrows, respectively. The T_is of the fast and the medium components are indicated in parentheses.

this case (note that the polarization angles are different by 50°). The small variation in the intensity between $\theta_{\rm des} = \pm 25°$ is probably due to errors in estimating the photo-irradiated area mentioned above. It is seen that the P_1 intensity is more sensitive to $\theta_{\rm des}$ than the P_2 intensity, indicating that the angular distribution of the former is narrower than that of the latter. The ratios of the fluxes of P_1 to P_2 were 0.92, 0.15, 0.93, and 0.04 at $\theta_{\rm des} = -25°$, 0°, 25°, and 45°, respectively. Figure 4 gives an angular plot of the desorption fluxes of P_1 and P_2. The fitting of the angle-dependent photodesorption fluxes of P_1 and P_2 to a $\cos^n(\theta_{\rm des} - \theta_{\rm d})$ function gave $n \sim 20$ (with $\theta_{\rm d} = 25°$), and 1.7 (with $\theta_{\rm d} = 0°$), respectively. These are admittedly very rough values due to the small number of data points.

The $\theta_{\rm des}$ dependence of the photofragment N_2 in figure 3(b) shows remarkably different features compared to those of N_2O. The desorption fluxes of both Q_1 and Q_2 were highest at $\theta_{\rm des} = 0°$. Q_1 appears to be peaked more sharply than Q_2. The ratios of Q_1 to Q_2 are 0.70, 1.22, 0.59, and 0.22 at $\theta_{\rm des} = -25°$, 0°, 25°, and 45°, respectively. Figure 4(b) plots the desorption fluxes of Q_1 and Q_2. The fitting of the angle-dependent photodesorption fluxes of Q_1 and Q_2 to a $\cos^n(\theta_{\rm des} - \theta_{\rm d})$ function resulted in $n \sim 12$ and 5 (both with $\theta_{\rm d} = 0°$), respectively; which again are rather rough values. In order to get a feeling for the total percentages going into the various components, we have to integrate over those angular distributions in three dimensions. We have to assume rotational symmetry around the surface normal. Because of the small number of points the results will only be semi-quantitative estimates. However, it is clear that the main overall desorption product is N_2, with N_2O being only about half of it. As a further breakdown, the total amount desorbed as P_1 is less than a fifth of the total N_2O, while Q_1 and Q_2 have about equal shares of the total N_2.

As indicated, these TOF determinations rest on integrations over the entire desorbed layer. In order to see whether the various components evolve differently with decreasing coverage, we did some partial integrations. In figure 5 we display the shot dependence of TOF spectra of N_2O ($m/e = 44$) ac-

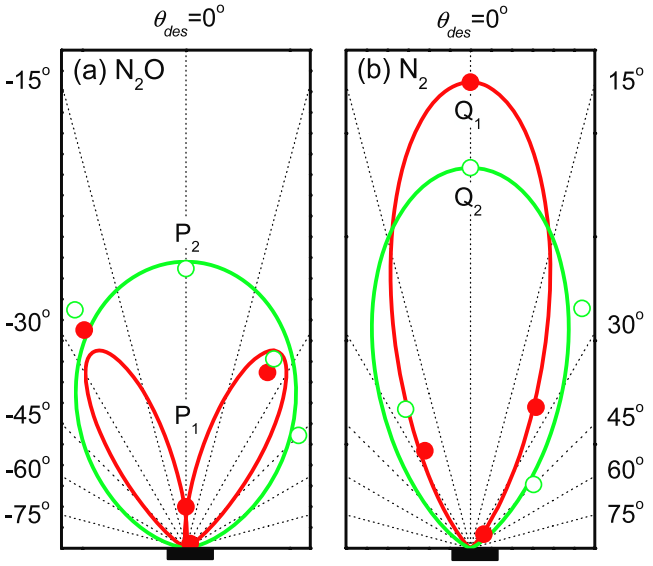

Figure 4. Polar plots of the desorption fluxes of the fast and the medium components of the TOF spectra in figure 3 of (a) N_2O and (b) N_2 photodesorbed from the N_2O monolayer on Ag(111) by 4.7 eV photons in p-polarization.

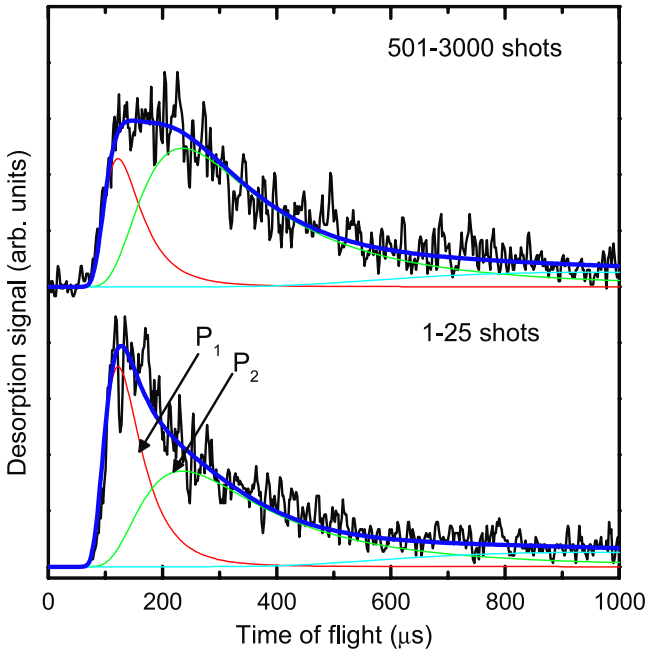

Figure 5. Dependence of TOF spectra of $m/e = 44$ on the total number of irradiating photons of 4.7 eV (p-polarization), at $\theta_{des} = -25°$. The P_1 component decays faster than the P_2 component.

cumulated for (a) 1–25 shots (about the highest 50% of the monolayer) and (b) 501–3001 shots (about the lowest 3% of the monolayer) measured at $\theta_{des} = -25°$ by irradiating with 4.7 eV photons in p-polarization. One laser shot corresponds to 1.1×10^{15} photons cm^{-2} on the surface. In this case, the curve fitting has been done independently for the two traces. The best fitting result shows that the spectral shapes of each speed component are almost the same as in figure 3(a); however, the relative intensities are significantly different. The fast component (P_1) is dominant at the low irradiances (i.e. high N_2O coverages) and becomes minor at the larger irradiances (low remaining coverages). This means that the P_1 component decays considerably faster than the P_2 component, which suggests that the origins and/or the photodesorption mechanism of the two components are different. This is consistent with the difference in their angular dependences shown in figure 4.

3.3. PID measurements of N_2O and N_2

In order to investigate the photoreaction mechanisms of N_2O, the kinetics of photoreactions of N_2O have been studied by measuring the evolution of the PID of N_2O and N_2 with irradiation. Figure 6 presents the PID signals of (a) N_2O and (b) N_2 on a logarithmic scale as a function of the accumulated number of photons at 4.7 eV in p-polarization for three different angular situations. Each data point is the integrated QMS signal of desorbed molecules for 2 ms after a single laser pulse and is normalized by the QMS sensitivity, the photon density on the sample, and the irradiated area. In the case of N_2 PID, the cracking contribution from N_2O is also subtracted.

While the PID intensities will contain the influence of the emission angle anisotropies demonstrated above, the relative PID signal decay (or increase) tracks the decrease (or increase) of the concentration of the adsorbed species which are its source; it is proportional to the photoreaction cross section (PCS). In the simplest case of a constant PCS, indicated by a declining straight line of the semi-logarithmic plot, the irradiation-induced decay of a single source species can be concluded. A changing slope indicates a changing PCS and/or source species; a signal increase must be due to the creation of a new source species or the growth in the coverage of an existing one. The angular dependence of the PCSs is determined by that of the surface absorbance or the photo-excitation probability, so that information on the photo-excitation and possibly also the mechanism of desorption can be hoped for.

The behavior shown in figure 6 is quite complex. In most cases the signals decay, but there are also increases (N_2 signals). The signal intensities and the slopes of both N_2O and N_2 PID signals strongly depend on the incident angle/desorption angle, but not always in a correlated way. For example, the largest intensity and the fastest decay of the N_2O signal was observed for $\theta_{des} = -25°$ ($\theta_{in} = 70°$), whereas for the N_2 signal this occurred at $\theta_{des} = 0°$ ($\theta_{in} = 45°$). In the case of N_2O PID, not only the PCS but also the ratio between the P_1 and P_2 components in the TOF spectra is angle-dependent. In figure 4(a), the P_2 component of the N_2O PID signal is dominant at $\theta_{des} = 0°$ ($\theta_{in} = 45°$) and $\theta_{des} = 45°$ ($\theta_{in} = 0°$), whereas the P_1 and the P_2 signals contribute almost equally to the data at $\theta_{des} = \pm 25°$ ($\theta_{in} = 20°$ and 70°). This can be used for the analysis of the polarization and incident angle dependences of PCSs to get information on the primary photo-excitation mechanisms, as will be discussed below.

The decay slopes of the N_2 signals are generally smaller than those of the N_2O signals. More importantly, and as already stressed, the N_2 signals initially rise and then decay.

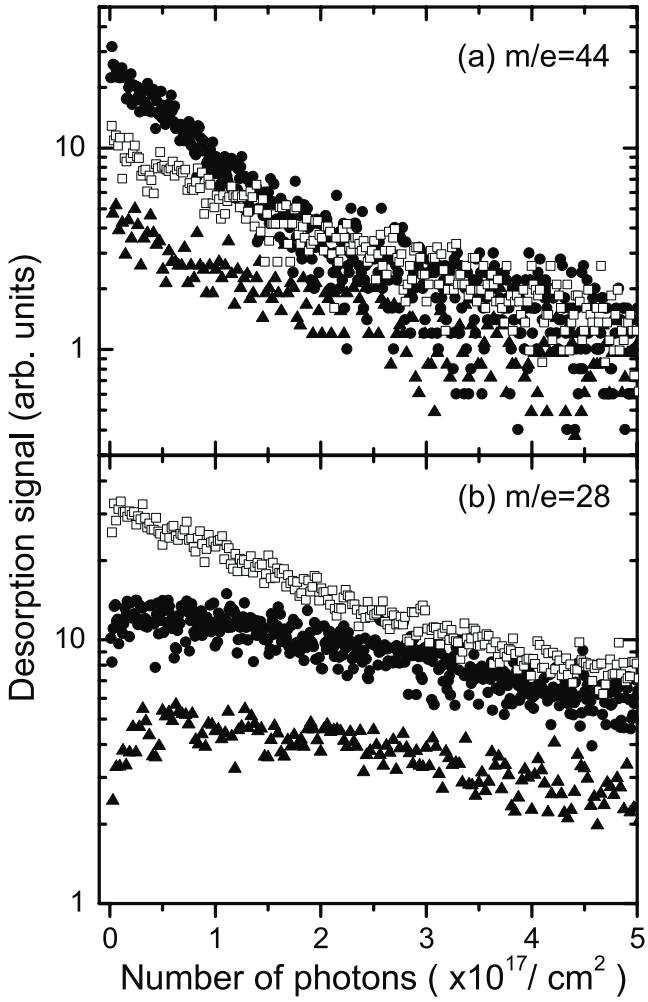

Figure 6. PID of the desorption signal at desorption angle $\theta_{\rm des} = -25°$ (filled circles), 0° (open squares), and 45° (filled triangles) for (a) $m/e = 44$ and (b) $m/e = 28$ by irradiating with 4.7 eV photons in p-polarization.

This is quite obvious at $\theta_{\rm des} = -25°$ ($\theta_{\rm in} = 70°$) and $\theta_{\rm des} = 45°$ ($\theta_{\rm in} = 0°$). For $\theta_{\rm des} = 0°$ ($\theta_{\rm in} = 45°$) the initial increase shows up in only a few data points, and without the other angles would not be believable; at the same time the maximum signal is by far the largest for this condition. The initial rise of the N_2 signal becomes more obvious at lower laser intensity (0.2 mJ cm^{-2} per shot) for all desorption angles, but the scatter of points increases as well (data not shown). While accurate determination of the cross section corresponding to this process is not possible due to the small number of points and their scatter, it is clearly an extremely fast process; it is essentially complete after the accumulation of about 10^{16} photons cm^{-2}. Fits to a kinetic equation with one increasing and one decreasing first order reaction are possible, but show strong scatter for the increase. An estimate for the PCS of the increase results in about 1×10^{-16} cm^2 (roughly the same for all three cases within a factor of 2) which shows that it must be more than 10–15 times faster than any other change. Even if extrapolating back to zero irradiation, these increases start from a nonzero initial signal value of desorbed N_2 which is highest for $\theta_{\rm des} = 45°$ ($\theta_{\rm in} = 0°$). The ratio of the extrapolated maximum signal value and the starting value is weakly angle-dependent, from about 4.0 ($\theta_{\rm des} = 45°/\theta_{\rm in} = 0°$) and 3.6 ($\theta_{\rm des} = -25°/\theta_{\rm in} = 70°$) to ~2.6 ($\theta_{\rm des} = 0°/\theta_{\rm in} = 45°$).

Before we discuss the information content of these angular variations, we have to arrive at a general picture. Obviously N_2O on the surface can photodesorb either molecularly—which is the weaker channel and can occur through two channels distinguished by different angular and PCS behaviors and different translational energies, i.e. by two different mechanisms and/or source species—or as the N_2 fragment; the latter is the main overall channel. It occurs to a certain extent from the start, i.e. from the unirradiated molecular layer, so that initially it must be due to direct photo-dissociation of adsorbed N_2O to gas phase N_2, in parallel to N_2O PID. The majority of N_2 PID, however, comes from a species which is formed by irradiation of the molecular layer. This latter, very fast process could be either dissociation to adsorbed N_2 (which may be made plausible by the fact that some adsorbed N_2 stays behind, see figure 2). On the other hand the fact that PID of N_2O continues after the very fast modification process is complete may be interpreted as meaning that this process is a conversion of the molecular layer. The latter possibility would also make the results better compatible with the simple TPD spectrum of the unirradiated layer. To be sure, such a TPD spectrum does not exclude the presence of more than one species, as long as they are in two-dimensional (2D) equilibrium during thermal desorption. So, even the thermal evolution could contain a conversion between species. While at our PID temperature (30 K) 2D equilibrium might not be maintained, here it could be photo-induced. We will come back to this below; here we conclude that our data suggest that we start with a layer essentially consisting of one N_2O species I, but there is a very fast photo-induced conversion of N_2O into another adsorption state II which accompanies the N_2O PID of species I and has a higher relative fragmentation probability. It occurs in parallel with decreasing overall coverage, i.e. species II may need more space per molecule. Of course there can also be the formation of adsorbed N_2 in parallel which then could show PID as well.

Thus, the photoreactions contributing to the PID signals of N_2O and N_2 can be summarized as follows:

$$N_2O(I) \rightarrow N_2O(g) \quad (1a)$$

$$N_2O(I) \rightarrow N_2O(II) \quad (1b)$$

$$N_2O(II) \rightarrow N_2O(g) \quad (1c)$$

$$N_2O(I) \rightarrow O(a/g) + N_2(g) \quad (2a)$$

$$N_2O(II) \rightarrow O(a/g) + N_2(g) \quad (2b)$$

$$N_2O(I/II) \rightarrow O(a/g) + N_2(a) \quad (3)$$

$$N_2(a) \rightarrow N_2(g). \quad (4)$$

We note that these are only the minimum steps possibly involved. There could well be an influence of the accumulated O and N_2 on the properties of the N_2O. However, we have no evidence of this, and increasing the complexity would not increase our understanding. So we do not include such possibilities in our discussion.

The initial N_2 signal is largest and its rise with irradiation smallest at $\theta_{des} = 0°$ (figure 6(b)). While we do not know the relative contributions of Q_1 and Q_2 as a function of coverage (figures 3 and 4 only give the integrated values for the entire coverage), we will show below that the PCS of Q_1 is considerably larger than that of Q_2 and thus dominates at high coverages, while Q_2 dominates at later stages of irradiation. We checked this by integrating the TOF spectra over small numbers of shots in the beginning and in later stages of photoreaction. A small increase of fast particles in the initial stages of desorption was compatible with the data, but due to the resulting very high signal/noise ratio this finding is not conclusive. Nevertheless, Q_1 is probably due to direct N_2 photo-dissociation of species II (and possibly also I), i.e. to reaction (2). This is also consistent with the higher relative increases by going from I to II at other angles, where generally Q_2 is stronger. This would be compatible with Q_2 being due to PID of adsorbed N_2 fragments (reaction (4)), but it is not possible to unequivocally prove these assignments.

3.4. Determination of photo-excitation mechanisms by incident angle, polarization, and photon energy dependences of photodesorption cross sections

We turn to the elucidation of the primary photo-excitation mechanisms involved in the photodesorption of N_2O and N_2. The main possibilities are indirect excitation, and direct excitation of the adsorbate by the incoming photons. Indirect excitation implies that the photons are absorbed in the substrate and create hot electrons which can be transferred to an adsorbate resonance. The created transient negative ion (TNI) is accelerated to the surface by the image force; when the transient electron is transferred back to the substrate, the neutral adsorbate finds itself too close to the surface and is kicked out [15]. Distinction is possible by the dependences on light incident angle and polarization [16] and also by the photon energy dependence of PCS, for the same process. To start with the latter, we have studied the photon energy dependences of the PCS of N_2O, derived from the exponential decay of the signal down to 50% of its maximum, at $\theta_{in} = 45°$ for 3.5 eV in p-polarization, 4.0 eV without polarization, and 4.7 eV in p-polarization. The extracted PCS values were 1.5×10^{-20}, 2.1×10^{-19}, and 5.7×10^{-18} cm^2, respectively. The photodesorption signal by 3.5 eV irradiation in p-polarization was hardly detectable with the QMS due to the low PCS, so an estimate was derived from comparison of the integrated TPD signals in pre- and post-irradiation (see figure 2) and the irradiating number of photons. The ratios of the PCS are obtained as 0.07:1.0:27 for these photon energies. On the other hand, the ratios of the effective absorbance at the Ag surface [17] at 3.5, 4.0, and 4.7 eV is 0.17:1.0:2.0 (taking into account the polarizations used). That is, there is a significant discrepancy between the effective absorbance of the Ag surface and the PCS of N_2O as a function of incident photon energy. This discrepancy makes the dominance of an indirect (substrate mediated) mechanism unlikely, and hints at the involvement of a direct desorption mechanism. To be sure, the absorbance gives the number of initially created hot electrons, and their

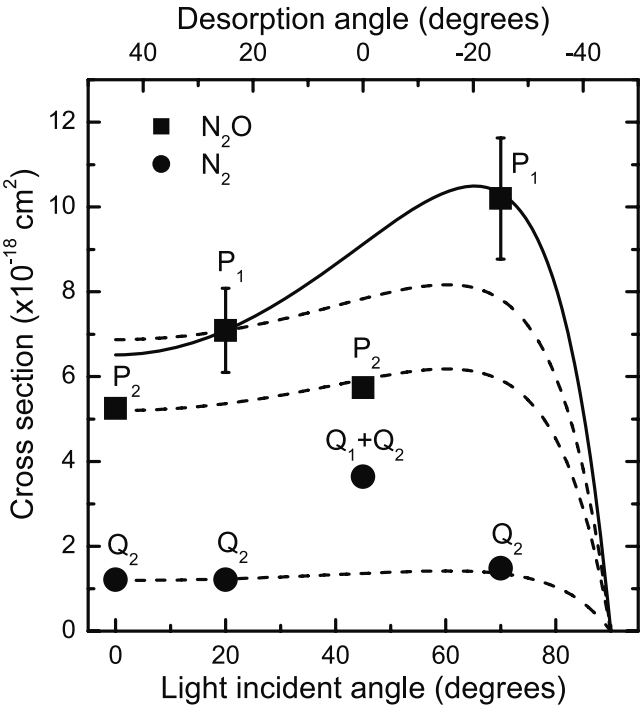

Figure 7. PCS of N_2O (solid squares) and N_2 (solid circles) as functions of light incident angle at 4.7 eV in p-polarization. The solid and the dashed curves show the best fit to the data sets of the photo-excitation probability [16] and the calculated surface absorbance, respectively. The captions P_1, P_2, Q_1 and Q_2 indicate the main speed components in the photodesorption signal at each corresponding desorption angle (see figure 3).

efficiency will depend on the energies of electron affinity level(s) (LUMOs) which will govern the desorption efficiency of a created hot electron—different LUMOs could exist and be accessible at 4.0 and 4.7 eV as in the case of N_2O on Si(100) [18]. Nevertheless, a factor 14 in efficiency would be necessary for 4.7 versus 4.0 eV photons to explain the numbers given above, which appears unlikely. The very small effect at 3.5 eV suggests that at most the low energy tail of a LUMO is accessible there, so we do not discuss the efficiency for this case; however, we can derive from it that if the indirect mechanism applies, the corresponding LUMO must be centered clearly higher than 3.5 eV above E_F, assuming the Ag(111) surface state close to E_F to be the starting level of the hot electron production. Also, direct excitation of the adsorbate should not be possible at this energy (see below).

So, while consideration of the energy dependence of PCSs makes the indirect mechanism unlikely and does hint at the validity of a direct mechanism, this is not conclusive. Fortunately, a clear picture is obtained from the polarization dependences at 4.7 eV, for which energy the best results are available. We derived PCS values by fitting single exponential decay functions to the PID data in the range between the maximum and the half maximum for N_2O, taking into account the dominant components as derived from the MS-TOF spectra. For N_2, the decay regions have been analyzed. Figure 7 plots the PCS values of N_2O and N_2 PID at 4.7 eV, assigning them to dominant components where possible.

The PCS data points of N_2O, shown as solid squares, are labeled by P_1 or P_2 based on the main speed component in the corresponding desorption angle at $\theta_{des} = 0°$ ($\theta_{in} = 45°$) and at $\theta_{des} = 25°$ ($\theta_{in} = 20°$) as in the angle-resolved MS-TOF measurements shown in figure 3. The P_2 component is dominant at $\theta_{des} = 0°$, as shown in figure 3(a), indicating that there the PCS is mainly determined by P_2. On the other hand, the contributions of P_1 and P_2 for $\theta_{des} = \pm 25°$ are comparable in the early stage, whereas the P_1 component decays much faster than the P_2 component as shown in figure 5. This implies that the PCS in this coverage range is mainly determined by P_1. The error bars shown for the N_2O PCS at $\theta_{des} = \pm 25°$ were estimated from the difference in the values when fitting was done between the maximum signal and 40% of the maximum (upper limit), and between the maximum and 60% of the maximum (lower limit). The PCSs of N_2 decays are plotted as solid circles. As in the case of the N_2O PCS, the data points are labeled by Q_1 and/or Q_2. Such grouping is useful because the measurement was done under the constraint $\theta_{des} = 45° - \theta_{in}$ (see figure 1). For example, at $\theta_{in} = 20°$ and 70°, i.e. at $\theta_{des} = \pm 25°$, the dependences on the incident angle θ_{in} can be extracted because of the symmetry in the desorption angle θ_{des}. Also, the comparison within the same groups, for example the N_2O PCS at $\theta_{in} = 0°$ and 45° (both for P_2), gives the incident angle dependence of the PCS. Note that the PCS value is independent of the absolute signals but only depends on the decay of the photodesorption signal. Therefore, the PCS is insensitive to the θ_{des} as long as signals with the same source species are measured.

Using these data we can answer the question about the primary excitation mechanisms. In all other work on N_2O photodesorption so far [5, 6, 18], the applicability of the indirect excitation mechanism was assumed or concluded. In such cases the polarization angle dependence of the PCS should follow the absorbance of the substrate. The dashed curves in figure 7 give such curves derived from the calculated absorbance for p-polarized light, A_p, of Ag [17], scaled in a way to best adjust them to the various data groups. It is seen that P_2 and Q_2 fit well to this assumption. On the other hand P_1 does not fit at all, due to the strong asymmetry between desorption angles of ±25°. This suggests the applicability of a direct excitation mechanism for P_1, i.e. the primary excitation takes place directly by photo-absorption in the adsorbate. In this case a correlation with the adsorbate geometry is expected, which will lead to a directionality of the transition dipole vector based on Fermi's golden rule. We find that for an angle of 74° between the transition dipole vector and the surface normal for the surface with $\geqslant C_3$ rotational symmetry [16] excellent agreement is reached (σ_p, solid curve). To be sure, this angle should not be taken too seriously, as considerable errors in the PCS values are expected. The error bars given at the experimental P_1 points have been derived as described above; errors in the correction for the angular dependence of the incident photon flux, which are difficult to estimate, are possible additionally. We conclude that angles between 65° and 80° would give acceptable fits, and more generally that a directional excitation applies for the underlying species. We will come back to this below.

We find that the very fast conversion of the adlayer from state I to state II appears to work at all polarization angles roughly equally (with large error, though); so it is probably due to indirect excitations. Also, it does not show up directly in the N_2O PID. It is tempting to identify the P_1 component with species I, which indeed disappears with the highest cross section, and P_2 with species II. However, one might then expect that the PCS of P_1 disappearance would be the same as that of I → II conversion, which is not the case. It could be that the entire coverage is not accessible to the conversion, so that part of the N_2O I state remains after the conversion.

So we conclude that at 4.7 eV P_1 is due to direct excitation, and P_2 as well as Q_2 are due to indirect excitation. A conclusion about the primary mechanism for Q_1 is not possible on these grounds, as we have no pure values and angular dependences for it. However, if the correlation of P_2 and Q_1 is correct, Q_1 is also due to indirect excitation. The PCS of N_2 at $\theta_{in} = 45°$, consisting of both the Q_1 and the Q_2 components, is about three times larger than the corresponding value of the A_p curve for the Q_2 only. This suggests that the PCS of Q_1 is much larger than that of Q_2. The maximum signal at $\theta_{des} = 0°$ is indeed due to Q_1 (see above). A semi-quantitative discussion for the PCSs of Q_1 and Q_2 will be given later. The very fast initial conversion is most likely due to indirect excitation.

We note that the PCS measured in s-polarization agreed with the model calculations for the direct and the indirect mechanisms, which corroborates the analysis. However, the data are not shown here for clarity, and because the differences in the curves between the direct and the indirect mechanisms are generally too small to determine the mechanism.

3.5. Origins and photodesorption mechanisms of N_2O and N_2 from N_2O/Ag(111)

In the MS-TOF spectra in figure 3 at least three speed components have been identified for both N_2O and N_2 photodesorbed from the monolayer of N_2O on Ag(111) at 4.7 eV. The slowest component in each case has been attributed to secondary processes, so it is not taken into account here. The fast and the intermediate components, which constitute intrinsic photodesorption, show differences in several characteristics, namely PCS, T_t, and direction and width of the spatial distribution of photoproducts. Also, their photo-excitation mechanisms differ, as has been shown in section 3.4. Here we summarize their characteristics and discuss their origins and possible photodesorption mechanisms.

3.5.1. Photodesorption of N_2O. The characteristics of the speed components P_1 and P_2 are compared in table 1.

Both components appear to exist from monolayer coverage on, but evolve differently with decreasing coverage (cf figure 5), since the PCS of P_1 is larger than that of P_2. The polarization dependence indicated that the photo-excitation mechanism of P_1 is direct, whereas that of P_2 is indirect. The first question to answer is whether the two components have different origins, i.e. different adsorption states and/or species, or whether they correspond to paths via

Table 1. Comparison of the fast (P_1) and the medium (P_2) components in photodesorption of N_2O from N_2O/Ag(111) at 4.7 eV in p-polarization.

Component	T_t (K)	Direction of photodesorption	n in $\cos^n \theta_{des}$	Photo-excitation mechanism	Reaction channel	PCS (10^{-18} cm^2)
P_1	3100	$\theta_{des} = \sim 25°$	20	Direct	(1*a*)	7.1[a] 10.2[b]
P_2	1100	$\theta_{des} = 0°$	1.7	Indirect	(1*c*)	5.3[c] 5.8[d]

[a] Measured at $\theta_{in} = 20°$. [b] Measured at $\theta_{in} = 70°$. [c] Measured at $\theta_{in} = 0°$. [d] Measured at $\theta_{in} = 45°$.

different photo-excitation, but derive from the same species. If they were derived from the same species, the PCS for their disappearance under irradiation would have to be the same. The strong difference in PCS clearly shows that different species are the sources of P_1 and P_2. It is possible, but not conclusive, that P_1 derives from the undisturbed layer (state I) while P_2 comes from state II. Since P_1 and P_2 exist from the start, the undisturbed layer would have to contain some state II. In the absence of geometrical information on the layer it is difficult to pinpoint these species, but we still consider it worthwhile to speculate in the light of the available information.

We have shown above that there is a very fast photo-induced conversion of the adsorbate layer from state I to state II. This conversion is faster than the desorption of P_1, but otherwise overlaps with the latter. The fact that P_2 and Q_2 exist from the start must mean that some II already exists in the undisturbed layer, even though a large part of this species is produced by irradiation. On the other hand this excludes that state II (and P_2) are due to the presence of photo-dissociation fragments like adsorbed O or N_2. So it is interesting to speculate on the possible existence of two adsorbed N_2O species, of which one dominates in the saturated undisturbed monolayer and the other is produced by irradiation and/or decreasing coverage. We also remember that species I is prone to direct excitation with angular preference, leading to directional PID of fast N_2O, while P_2 as well as the fragments and the fast conversion are most likely caused by indirect excitation.

The low binding energy and the very small energetic difference between monolayer and multilayer suggest mainly van der Waals bonding of N_2O. For low coverages this will be optimized by lying-down N_2O, while at higher coverages standing-up N_2O, with lateral van der Waals and multipole interactions, will be preferred. The latter could be oriented O- or N-end down. In other N_2O layers on transition metal surfaces, standing-up N_2O (inclined from the surface normal) has been seen [19]. No evidence for an O-end down species is known to us. Wu *et al* studied the adsorption structure of N_2O on Ag(110) with NEXAFS and concluded that N_2O is adsorbed to Ag(110) through the terminal N-end down [20]. So we make the tentative assumption that state I is such a layer of dense, upright but likely inclined molecules. The findings in other N_2O layers makes the N-end down orientation more likely than O-end down, but we cannot exclude the latter (in fact the direct photodesorption of N_2 upon its production due N_2O photodissociation, reactions (2*a*) and (2*b*), would appear easier for that geometry). The upright geometry would explain the directionality of excitation and PID; the high density obtainable in this geometry would make it the dominant species at high coverages. Species II could then be a lying-down species which becomes possible when the coverage of the layer is decreasing. The first species would be stabilized by lateral interactions, with the tilt deriving from interaction of the uneven charge distributions along the N_2O molecules. The second species would be lying down to optimize the van der Waals interaction with the substrate. It should be noted that such a layer with two possible configurations is well compatible with the pre-irradiation TPD with its single, zeroth order peak, if at TPD temperatures these species were to readily interconvert as a function of coverage at desorption temperature. Such 2D equilibrium is well known to lead to this kinetics [21, 22]. The presence of some lying-down species in our starting layers appears possible in view of our preparation procedure in which the sample was dosed with N_2O at a few kelvin lower than the desorption temperature from the first layer, in the interest of exclusion of second layer species. This might not have produced a truly saturated monolayer containing only one species.

This admittedly rather speculative picture becomes more acceptable with regard to the characteristics of the various species if we assign I/P_1 to the standing-up species and II/P_2 to the lying-down one. Then the different photo-excitation paths and the two distinctly different desorption angles are naturally explained.

The inclined desorption angle of P_1 makes this the most interesting species, despite its small branching ratio. To our knowledge this is the first reported case of inclined desorption for a weakly bound molecule. Desorbing fragments often show directed beams (best investigated for ions, by the 'ESDIAD' method [23]) due to the directionality of the broken bonds, and chemisorbed molecules with strong directionality could lead to similar effects. However, this is more difficult to conceive for a weakly bound species on an almost uncorrugated surface, even if the molecule is tilted by lateral interactions. As for N_2O, Matsumoto and co-workers observed off-normal photodesorption of N_2 from N_2O on Si(100) at 5.0 and 6.4 eV [24]. In this case, the N_2O is chemisorbed and the interaction between the N_2O and oxygen atoms was thought to give a surface-parallel momentum. However, off-normal signals were not observed in the PID of N_2O and N_2 from N_2O/Pt(111) studied by the same authors [24]. In contrast, Kummel and co-workers observed off-normal PID of oxygen atoms emitted from N_2O/Pt(111) irradiated with

Table 2. Comparison of the fast (Q_1) and the medium (Q_2) components in photodesorption of N_2 from N_2O/Ag(111) at 4.7 eV in p-polarization.

Component	T_t (K)	Direction of photodesorption	n in $\cos^n \theta_{des}$	Photo-excitation mechanism	Reaction channel	PCS (10^{-18} cm^2)
Q_1	2200	$\theta_{des} = 0°$	12	N/A	(2*b*)	<3.6[a] 1.2[b]
Q_2	600	$\theta_{des} = 0°$	5	Indirect	(4)	1.2[c] 1.5[d]

[a] Measured at $\theta_{in} = 45°$. [b] Measured at $\theta_{in} = 0°$. [c] Measured at $\theta_{in} = 20°$. [d] Measured at $\theta_{in} = 70°$.

6.4 eV photons [25]. They concluded that oxygen atoms (both $O(^3P)$ and $O(^1D)$) are emitted along the molecular axis of the parent N_2O molecule tilted at 35° from the surface plane [19]. However, PID of molecular N_2O tilted from the surface normal was not reported. Importantly, N_2O PID on Pt(111) appears to work via the substrate mediated excitation mechanism [6, 26], in contrast to our P_1 component. Also note that the N_2O is bound on Pt(111) more strongly than on Ag(111). If we accept the notion of a standing, tilted species, then a possible explanation of the inclined desorption could be a kind of 'channeling' of the desorption direction of a leaving molecule in a collectively tilted island. We shall come back to this after discussing the probable desorption mechanism, in connection with the excitation involved, and the angular behavior.

In view of the weak bonding of even the standing-up and probably tilted N_2O in the monolayer, the molecular properties are not expected to be changed drastically from the free molecule. The main effect of adsorption on the low-lying electronic excitations will be a redshift of the necessary energy, due to screening by the substrate, by which the HOMO moves up energetically and the LUMO moves down. As the lowest excitation of the free molecules needs about 5.2 eV [27–29], our 4.7 eV excitation would not suffice (and 4.0 eV even less so) to directly excite the molecule without the screening-induced gap narrowing. In the free molecule the lowest absorption band is broad and contains many excitations, complicated by the existence of conical intersections [28, 29]. It has been concluded from calculations that the lowest three excitations need assistance from the bending of the linear molecule [28, 29]; the resulting angular dependence is complex. These excitations lead to photo-dissociation into ground state N_2, which is vibrationally cold and rotationally hot, and electronically excited $O(^1D)$. There are contributions from both perpendicular and parallel excitations. This makes quantitative conclusions from the angular behavior of the photo-excitation probability demonstrated above difficult. Nevertheless, its directionality as well as the (different) directionality of desorption strengthens the argument for a tilted, dense species as the source of P_1.

The P_2 component, on the other hand, is peaked in the surface normal with a T_t of 1100 K, which is between the values (1700 and 810 K) observed for N_2O photodesorption from Pt(111) [26]. Our angle-of-incidence dependence of the PCS suggests that this component stems from indirect excitation of N_2O by hot electron attachment. This is well compatible with its PID angle dependence. Thus, PID of the P_2 component can be explained by the TNI mechanism of Zimmerman and Ho [15], as in the Pt(111) case. The spatial distribution of P_2 points into the surface normal, but is rather broad ($n = 1.7$). This may suggest scattering of N_2O^- by neighboring adsorbates. A lying-down N_2O species which optimizes the van der Waals interaction with the surface in a dilute layer would well fit in. Detailed investigation of the adsorbate geometry, which is not possible in our apparatus, would be very helpful.

We cannot say much about the conversion process since it is so fast that detailed kinetics could not be carried out. Indirect excitation is likely. Also, since a lying-down molecule requires more space than one standing up, the reduction of coverage by irradiation is certainly an important prerequisite of the conversion and may partly explain the different cross sections.

3.5.2. Photodesorption of N_2. The features of the Q_1 and Q_2 components in N_2 photodesorption from N_2O/Ag(111) are summarized in table 2. Both components are peaked in the surface normal, similar to the case of N_2O/Pt(111) [25, 26]. However, the T_ts, the PCSs, and the widths of spatial distributions are different for Q_1 and Q_2.

There are at least three PID channels of N_2. The first two are direct photo-dissociation of N_2O of either species I or II, emitting N_2 into the gas phase as reactions (2*a*) and (2*b*). The third is PID of the photoproduct N_2 adsorbed on the surface as reaction (4), which has been produced by photo-dissociation without fragment desorption in reactions (3).

The Q_1 component, which dominates at $\theta_{des} = 0°$ and shows only a small initial growth (but by far the largest maximum signal), is probably due to photodesorbed N_2 by direct photo-dissociation of species II. Unfortunately, due to the low signal we could not obtain an angular dependence of Q_1 on the light vector; we only know that its angular emission is directed into the surface normal. Also, the different PCSs appear to exclude a connection between P_2 and Q_1 at first sight (figure 7). Closer examination shows, however, that this connection is indeed possible. The PCS for N_2 at normal emission (figure 7) contains contributions from both Q_1 and Q_2. If the species and primary excitation leading to $Q_1 - N_2$ are identical to those leading to $P_2 - N_2O$, then the two PCSs must be equal. This is in fact consistent with the values shown in figure 7. The N_2 PCS of 4×10^{-18} cm^2, measured at $\theta_{in} = 45°$ ($\theta_{des} = 0°$), is a composite value containing contributions from the decrease of Q_1 and Q_2. If we assume that the PCS of Q_1 is equal to that of P_2 (N_2O), σ_{P2} (6×10^{-18} cm^2), and

that of Q_2 can be obtained by interpolation of the (barely angle-dependent) PCS at the other angles (leading to about 1.5×10^{-18} cm^2), then roughly equal relative contributions of Q_1 and Q_2 lead to the measured composite PCS by weighted averaging. Indeed, the signal ratio of Q_1 to Q_2 is 0.55:0.45 at $\theta_{in} = 45°$ in figure 3(b). While this is no proof that the sources and primary excitations leading to $Q_1 - N_2$ and $P_2 - N_2O$ are identical, this is well compatible with the data.

As for the probable mechanism of this dissociative PID, it is interesting to note that negative charging of N_2O on catalysts (albeit there by interaction with transition metal ions) does lead to dissociation into N_2 and O [30, 31]. So the formation of a transient negative ion by hot electron transfer into the N_2O LUMO could conceivably lead to dissociation. The fragments can separate from the surface, leading to the Q_1 component discussed here, or stay on the surface, leading to adsorbed N_2.

Concerning the Q_2 component, we recall that it is dominating at $\theta_{des} = \pm 25°$ and 45°. At these angles the initial signal growth with irradiation is strong. This could be due to the accumulation of the photoproduct N_2 by reaction (3), or to a higher direct dissociative PCS for species II compared to species I. The data do not allow a clear decision. The only exclusion possible is that this component cannot be connected to P_1/I because of the very different PCS values. Also direct photo-dissociation of species I would be expected to lead to angular focusing as for P_1. However, if Q_1 is due to direct photo-dissociation it is more likely that Q_2 stems from desorption of adsorbed fragment N_2. Its T_t (600 K), much higher than the substrate temperature, indicates that substrate heating by laser irradiation cannot be its cause. Nonthermal photodesorption of N_2 from Ag(111) by infrared irradiation (1.17 eV) has been reported by White *et al* [32]. They suggested that 'physisorbed adsorbates can couple directly to the nascent-phonon distribution or the nascent electron–hole pairs in the photo-excited substrate without heating of the surface'. In their measurements the T_t of N_2 photodesorbed from Ag(111) at ∼30 K was ∼100 K. However, the T_t of Q_2 is six times higher. This shows that the photodesorption mechanism of Q_2 is likely to be different from IR induced desorption as proposed by White *et al* [32]. We also note that the N_2 species produced here by photo-dissociation is probably different from that of [32], which was pure N_2, because of the co-adsorbed O atoms (and N_2O), and as our way of creating it might lead to different bonding.

Injection of a hot electron into the LUMO of weakly chemisorbed N_2 corresponding to its $2\pi^*$ antibonding orbital located from ∼0.5 to ∼3 eV above the vacuum level with a peak at ∼1.5 eV [33, 34] can lead to photodesorption of the N_2 (a) by the TNI mechanism. This state is accessible to hot electrons excited in the Ag substrate by photon absorption, similar to the P_2 N_2O state. Interestingly, Harrison and co-workers have argued that this works only for chemisorbed but not physisorbed N_2, since for the latter species the LUMO is above the vacuum level [35, 36]. If this is correct, the species produced by photo-dissociation on Ag(111) would have to be chemisorbed. This is conceivable, since a probably necessary activation energy can likely be provided by the photo-dissociation event. Also, thermal desorption of physisorbed N_2 is expected below 40 K, while figure 2 shows it to occur up to 60 K.

Summarizing, the fast N_2 component (Q_1) probably originates from direct photo-dissociation of N_2O(II), most probably via the P_2 excitation. The slower component (Q_2) may mainly result from desorption of N_2 (a) via the TNI mechanism, which is produced by photo-dissociation of N_2O, possibly also via the P_2 excitation. It is worth mentioning that the T_ts of both components are much lower than that observed in photodesorption of N_2 from NO dimers on Ag(111) (T_t = 5700 K) [11], where very special dynamics appear to operate.

4. Conclusions

We have found that a monolayer of N_2O on Ag(111) is photoreactive at photon energies ⩾3.5 eV, with molecular desorption occurring with a very low cross section even at 3.5 eV, while 4 eV and more are necessary for efficient molecular desorption and dissociation. This leads to both desorbing N_2 and adsorbed N_2 which can then also be photodesorbed. These processes have been investigated in detail by polarization-dependent photo-irradiation at 4.7 eV. Integrated over all paths, the photofragment N_2 is the dominant species.

The photodesorbed N_2O shows two distinct desorption dynamics which must be attributed to two different ad-species, although the pre-irradiation TPD shows a single molecular desorption peak. The fastest speed component (P_1, T_t = 3100 K) is directed in an off-normal direction (∼25°) with a sharp angular distribution. This appears to be the first example of off-normal molecular photodesorption from a monolayer of homogeneous adsorbates on a flat metal surface. A slower component (P_2, T_t = 1100 K) is desorbed into the surface normal with a relatively broad angular distribution. Based on the angle-of-incidence dependence of the photodesorption cross sections (PCSs), it is concluded that the P_1 component stems from direct photo-excitation of one adsorbate species, whereas the P_2 originates from indirect excitation of another ad-species by hot carriers from the substrate. We speculate that the first species might be adsorbed in a tilted standing-up configuration, while the second species might be lying down. A very fast photo-induced conversion from the first to the second species, when the coverage decreases by PID, shows up in the N_2 signal.

The N_2 PID signal also consists of two distinct speed components, which are both directed into the surface normal, with different angular widths. The faster speed component (Q_1, T_t = 2200 K) probably results mainly from direct photo-dissociation of N_2O adsorbed on the surface. The second component (Q_2, T_t = 600 K) is probably mainly due to desorption of an N_2 adsorbate produced by N_2O photo-dissociation. We discuss possible desorption paths for all species.

Acknowledgments

We acknowledge financial support from the Deutsche Forschungsgemeinschaft within priority program SPP1093

(Dynamik von Elektronentransferprozessen an Grenzflächen), the German–Israeli Foundation (Dynamics of Electronic Processes in a Confined Environment), the Fonds der Chemischen Industrie, and the NEDO International Joint Research Grant on Photon and Electron Controlled Surface Processes.

References

[1] Horino H, Liu S W, Hiratsuka A, Ohno Y and Matsushima T 2001 *Chem. Phys. Lett.* **341** 419
[2] Li Y X and Bowker M 1996 *Surf. Sci.* **348** 67
[3] Henderson M A, Szanyi J and Peden C H F 2003 *Catal. Today* **85** 251
[4] Sawabe K and Matsumoto Y 1992 *Chem. Phys. Lett.* **194** 45
[5] Kiss J, Lennon D, Jo S K and White J M 1991 *J. Phys. Chem.* **95** 8054
[6] Sawabe K and Matsumoto Y 1993 *Surf. Sci.* **283** 126
[7] Schwaner A L, Mahmood W and White J M 1996 *Surf. Sci.* **351** 228
[8] Vondrak T, Burke D J and Meech S R 2000 *Chem. Phys. Lett.* **327** 137
[9] Behm R J and Brundle C R 1984 *J. Vac. Sci. Technol.* A **2** 1040
[10] Brown W A and King D A 2000 *J. Phys. Chem.* B **104** 2578
[11] Kim K H, Watanabe K, Menzel D and Freund H J 2009 *J. Am. Chem. Soc.* **131** 1660
[12] Watanabe K, Kim K H, Menzel D and Freund H J 2007 *Phys. Rev. Lett.* **99** 225501
[13] Mulugeta D, Kim K H, Watanabe K, Menzel D and Freund H J 2008 *Phys. Rev. Lett.* **101** 146103
[14] Schlichting H and Menzel D 1993 *Rev. Sci. Instrum.* **64** 2013
[15] Zimmermann F M and Ho W 1995 *Surf. Sci. Rep.* **22** 127
[16] Zhu X Y, White J M, Wolf M, Hasselbrink E and Ertl G 1991 *Chem. Phys. Lett.* **176** 459
[17] Kidd R T, Lennon D and Meech S R 1999 *J. Phys. Chem.* B **103** 7480
[18] Kato H, Lee J, Sawabe K and Matsumoto Y 2000 *Surf. Sci.* **445** 209
[19] Avery N R 1983 *Surf. Sci.* **131** 501
[20] Wu T Q, Tang J C and Li H Y 2006 *Appl. Surf. Sci.* **252** 7837
[21] Schlichting H and Menzel D 1992 *Surf. Sci.* **272** 27
[22] Widdra W, Trischberger P, Friess W, Menzel D, Payne S H and Kreuzer H J 1998 *Phys. Rev.* B **57** 4111
[23] Madey T E, Ramaker D E and Stockbauer R 1984 *Annu. Rev. Phys. Chem.* **35** 215
[24] Matsumoto Y, Lee J W, Kato H and Sawabe K 1994 *Laser Techniques for Surface Science*; *Proc. SPIE* **2125** 303
[25] Masson D P, Lanzendorf E J and Kummel A C 1995 *Phys. Rev. Lett.* **74** 1799
[26] Matsumoto Y, Sawabe K and Lee J 1993 *Laser Techniques for State-Selected State-to-State Chemistry*; *Proc. SPIE* **1858** 378
[27] Selwyn G S and Johnston H S 1981 *J. Chem. Phys.* **74** 3791
[28] Brown A, Jimeno P and Balint-Kurti G G 1999 *J. Phys. Chem.* A **103** 11089
[29] Daud M N, Balint-Kurti G G and Brown A 2005 *J. Chem. Phys.* **122** 054305
[30] Stirling A 1998 *J. Phys. Chem.* A **102** 6565
[31] Ritter D and Weisshaar J C 1990 *J. Phys. Chem.* **94** 4907
[32] Rao R M, Beuhler R J and White M G 1998 *J. Chem. Phys.* **109** 8016
[33] Demuth J E, Schmeisser D and Avouris P 1981 *Phys. Rev. Lett.* **47** 1166
[34] Rous P J 1995 *Phys. Rev. Lett.* **74** 1835
[35] Zehr R, French C, Haynie B, Solodukhin A and Harrison I 2000 *Surf. Sci.* **451** 76
[36] Zehr R, Solodukhin A, Haynie B C, French C and Harrison I 2000 *J. Phys. Chem.* B **104** 3094